JCTC Journal of Chemical Theory and Computation

The Interaction of Coinage Metal Clusters with the MgO(100) Surface

Giovanni Barcaro and Alessandro Fortunelli*

Molecular Modeling Laboratory, Istituto per i Processi Chimico-Fisici (IPCF) del C. N. R., via V. Alfieri 1, 56010 Ghezzano (PI), Italy

Received March 22, 2005

Abstract: The results of a systematic study of the interaction of small coinage metal clusters (M_n, $n = 1-3$) and extended deposition (one and two MLs; ML = monolayer) with the regular and locally defected (F_s center and divacancy) neutral MgO(100) surface are presented. The calculations have been performed at the DFT level employing plane waves as a basis set and using a gradient-corrected exchange-correlation functional (PW91). The adhesion energy along the group follows a trend that can be rationalized in terms of the strength and "stickiness" of the metallic bond, electrostatic polarization effects, and chemical interactions. Coinage metal dimers and trimers are absorbed on the regular surface in an upright position with little modification with respect to the gas-phase structure and can easily diffuse from site to site (in the case of trimers, also because of their fluxional character). In the case of extended deposition, the adhesion energy increases when passing from one to two MLs because of a "metal-on-top" stabilization mechanism. Neutral localized defects on the surface such as the F_s center (generated by a missing O atom) and the double vacancy (generated by a missing MgO dimer) act as strong trapping centers for small clusters and remarkably increase the adhesion of metal slabs to the surface in the case of extended deposition. At variance with the F_s center, the double vacancy induces a strong structural and energetic modification of the surrounding oxide lattice, varying also as a function of the metal deposition. A peculiar structural rearrangement consisting of the segregation of the metal slab into "islands" on the surface is observed in the case of one ML Cu and (to a lesser extent) Au.

1. Introduction

Transition metal nanoclusters have gained increasing attention in science and application in the past several years as a result of the observation of properties that are unique to the nanoscale domain.[1−4] From a technological point of view, the process of stabilization of the metal clusters by coating with surfactants or through absorption on a substrate is an essential step to exploit the many potential applications of these materials. For this reason, a considerable experimental and theoretical effort has been dedicated to the study of the interaction and structural modifications induced in the metal aggregate by the presence of a supporting substrate[5−29] or surfactant and solvent molecules.[33−35] Moreover, the experimental conditions of the stabilization process can be tuned in order to induce the formation of supraorganized structures of single nanocluster units.[4,34−36] From a theoretical point of view, the characterization of transition metal clusters absorbed upon a supporting substrate has mainly concentrated on the study of static structures and has rarely dealt with the mechanism of nucleation and growth (see, however, refs 29−32, 100). Furthermore, despite the many contributions to this field, previous theoretical work lacks a systematic homogeneous comparison between elements belonging to the same group. The aim of the present paper is to provide such a comparison for the metals belonging to the group IB and the MgO(100) surface. Attention will be concentrated on the interaction of small coinage metal clusters and extended

* Corresponding author. Tel: +39-050-3152447, e-mail: fortunelli@ipcf.cnr.it.

10.1021/ct050073e CCC: $30.25 © 2005 American Chemical Society
Published on Web 08/12/2005

deposition with the regular or localized defected neutral MgO(100) surface. These systems present several elements of interest. On one hand, nanoclusters formed by coinage metals (Cu, Ag, and Au), both mono- and bimetallic, exhibit interesting optical, electronic transport, and catalytic properties, both in the gas phase and when stabilized by a substrate or by surfactant molecules.[33,37−44] On the other hand, the MgO(100) surface both is experimentally well-characterized and has technological (e.g., catalytic) applications.[3,45] Moreover, its theoretical description is simplified by the fact that this surface does not present the complications associated with surface reconstruction, MgO being a simple ionic solid and the (100) surface being a nonpolar one. In discussing the results, we will highlight analogies and differences in the behaviors of the coinage metals in order to extract information on both static and dynamic properties of the metal/MgO interaction. These results can form the basis for (a) a comparison with experimental data on the growth of coinage metal clusters and thin films, (b) building semiempirical metal/oxide interaction potential, which can be used in the simulation of actual growth processes, and (c) improving other simplified (for example, thermodynamic) theoretical models.

Previous Work. During the past few years, several theoretical approaches have been used to study transition metal nanoclusters. First principles calculations have been performed on small metal aggregates in order to determine the minimum energy structure and structure/property relationship as a function of cluster size.[46−55] Numerical procedures based on genetic algorithms for single and bimetallic structures using atom−atom pair potentials[56] or many-body potentials[56−64] have been used to investigate a broader range of cluster sizes. Focusing on transition metal clusters supported on magnesia surfaces, in the past 10 years, a wealth of results has been collected on the interaction of single metal atoms on the regular and defected sites of the MgO(100) surface.[65−69] The extended and localized defected sites of the MgO surface have attracted remarkable attention because of their intrinsic chemical and physical properties[70−84] and because they can act as trapping centers for metal atoms absorbed on the oxide surface.[67,85] The results of such calculations have demonstrated that the choice of the model influences the description of the system[86] and that the metal/surface interaction changes primarily as a function of the electronic configuration and the dimensions of the metal species considered. For example, the coinage metals, which are characterized by a filled d shell plus an outer, unpaired s electron, are weakly bound to the surface (with adhesion energy less of 1 eV) because of the Pauli repulsion with the electron density of the oxide.[67] The catalytic properties of systems formed by a single atom or small clusters absorbed on the regular and defected MgO surfaces have been studied by monitoring the absorption of probe molecules on the metal atoms.[39,78,87−92] The real-time monitoring of cluster growth on MgO offered by GISAXS[9] has further promoted the study of the minimum structure configurations of metal clusters and extended deposition on regular and defected MgO(100) surfaces in order to extract information on the mechanism of nucleation and growth and on the modifications in structure and properties induced in the metal aggregate by absorption on the oxide surface.[42,65,93−102] In particular, the study of the small clusters and extended deposition of coinage metals (Cu and Ag) has been performed through standard DFT calculations,[103−109] Car Parrinello calculations,[29−32] and a thermodynamic model describing the metal/oxide system in terms of a solid solution.[83,110] The general conclusion is that the Cu and Ag interactions with the regular surface are weak. Small clusters are absorbed in an upright position with negligible modifications with respect to the gas-phase structure and are able to diffuse over the surface through leapfrog, twisting, and rolling movements. In the case of extended deposition, there is an increase of the adhesion energy to the surface when passing from one to two MLs, thanks to a polarization stabilization mechanism. Classical molecular dynamics calculations of the growth process have, until now, been performed only for Pd clusters absorbed on the regular MgO surface[111−113] thanks to the development of a specific metal/oxide potential, fitted on the results of first-principle calculations. An analogous potential is still lacking for the coinage metal clusters. One of our goals is to provide the theoretical input data for the construction of such a potential, accounting not only for the interaction with the regular surface sites but also for the interaction with localized neutral vacancies.

2. Computational Details

All the calculations reported here were performed at the DFT level employing the PWscf (Plane-Wave Self-Consistent Field) computational code[114]. For each atom, the interaction between the outer-shell electrons and the positive nucleus is shielded by a pseudopotential accounting for the influence of the inner-shell electrons. All the calculations were performed spin-unrestricted. The PW91 exchange-correlation functional was employed,[115] which is a gradient-corrected density functional. From previous experience, we do not expect qualitative changes when using other gradient-corrected density functionals. However, it has been shown (see, e.g., ref 86) that the use of hybrid density functionals produces an overall (roughly constant) reduction in the metal/surface interaction energies.

The geometry optimizations were stopped when maximum force on the atoms was less than 4×10^{-4} au. All of the configurations reported here were checked to insure that they were local minima in the energy hypersurface. Few saddle point configurations can be found among those reported in the Supporting Information.

The dimensions of the plane-wave basis set are determined by the kinetic energy cutoff, which was fixed at the value of 40 Ry for all of the calculations. The *k*-point sampling of the Brillouin zone was changed according to the conductive properties of the metal deposition absorbed on the oxide. In the case of the deposition of one and two ML metallic slabs, which are conductive (small energy gap between the HOMO and LUMO energy), it was necessary to increase the number of *k* points per unit cell and to apply a procedure of Gaussian smearing (a value of 0.002 Ry was chosen as the smearing parameter for every sampled point of the Brillouin zone).

The dimensions of the unit cell were modified according to the metal deposition, as specified in detail in the following sections. A common aspect of all the different cells employed is that the oxide surface was built by positioning the Mg and O atoms at the equilibrium lattice positions of the MgO rock-salt structure (isomorphic with NaCl) and cutting this bulk structure along 100 directions. The O atoms on the surface are surrounded by four Mg surface atoms plus one Mg bulk atom and vice versa. The distance between the two opposite surface layers of the oxide slab is about 10 Å. The lattice constant of the oxide corresponded to the experimental value of 4.208 Å (implying a Mg−O distance of 2.104 Å). When the oxide bulk structure is relaxed at the DFT level, the equilibrium lattice constant is overestimated by about 2%. However, the metal/surface interaction energies do not qualitatively vary when using the DFT-optimized lattice constant (unpublished results).

In the calculations involving the regular (undefective) oxide surface, the MgO structure was left frozen and only the atomic coordinates of the metallic atoms absorbed on the surface were optimized. In the case of the defected surfaces, we have followed two different approaches. In the case of a single F_s vacancy, we have relaxed the oxide lattice around the defect in the absence of metal atoms; such a structure has then been frozen, allowing only the relaxation of the metal atoms absorbed upon it. We have checked in test cases that there is a negligible difference between the results obtained following this approach and the results obtained allowing a further relaxation of the oxide surface upon metal deposition. In the case of the double vacancy (which can be thought of as a desorption of a neutral MgO dimer in the 100 direction), the relaxation plays a very important role,[100] and to obtain an accurate estimate of the metal absorption energies, we allowed a complete relaxation of the atoms of the defected oxide and all the metal atoms. For this reason, the calculations involving the double vacancy are, computationally, rather intensive.

3. Results and Discussions

This section is divided into three subsections: absorption (I) on the regular terrace of the MgO(100) surface, (II) on a neutral oxygen vacancy (F_s center), and (III) on a neutral divacancy

Each of these subsections will separately treat the case of the absorption of (A) isolated metal atoms, (B) metal dimers, (C) metal trimers, and (D) extended depositions (one and two MLs)

For each system, we report four values of energy:

(1) The Absorption Energy (E_{int}). This quantity is calculated by subtracting the ground-state energy of the isolated oxide and the isolated metal atoms from the value of the total energy of the system. The absorption energy corresponds to the energy gain achieved by moving the single cluster constituents from infinite distance to the equilibrium distance characterizing a particular configuration.

(2) The Adhesion Energy (E_{adh}). This quantity is calculated by subtracting the energy of the oxide surface and that of the metal cluster, both frozen in the interacting configuration, from the value of the total energy of the system.

(3) The Oxide Surface Distortion Energy (ΔE_{MgO}). This quantity corresponds to the "distortion energy" of the oxide surface. It is calculated by subtracting the energy of the oxide surface in the interacting configuration from the ground-state energy of the surface.

(4) The Metal Cluster Distortion Energy (ΔE_{met}). A quantity analogous to the previous one but for the metal cluster.

We report only a selection of the configurations that have been considered. Additional data can be found in the Supporting Information.

I. Interaction of Coinage Metal Clusters with the Regular Terrace of the MgO(100) Surface. As anticipated before, for this system, no relaxation of the MgO surface was allowed ($\Delta E_{MgO} = 0$). This is consistent with the experimental observation that this surface does not reconstruct. We optimized only the coordinates of the metal atoms because the surface structure modification induced by the absorbed metal is negligible.

I.A. Isolated Adatoms. The absorption of the isolated adatoms has been studied modeling the (100) terrace by a three-layer slab, each containing four Mg atoms and four O atoms (a five-layer-slab model gave essentially identical results). The minimum distance between metal atoms in neighboring unit cells was larger than 6 Å; this distance is sufficiently large to make the interaction between the metal atoms negligible.

Three characteristic sites of absorption have been considered: (1) the O^{2-} ion, (2) the Mg^{2+} ion, and (3) the hollow site (see Figure 1a). The results of the interaction energies are reported in Table 1. In Figure 1 of the Supporting Information, the absorption energies on the O^{2-} ion are reported for the three metals as functions of the metal−surface distance. The interaction is stronger for Cu and Au atoms, while it is weaker for Ag;[68] all three metals interact more strongly with the O^{2-} ion site of the surface, while the Mg^{2+} ion is the site characterized by the smallest value of adhesion energy.

The tendency of absorbing atop the O^{2-} site is a common trend among transition metal atoms.[32,65,66] The stabilizing contributions of the interaction can be of three types: (1) chemical bonding, (2) electrostatic stabilization, and (3) dispersion interactions. The Pauli repulsion between the metal cloud and the electronic density of the surface represents, instead, the mainly destabilizing contribution. This repulsion is certainly stronger for the coinage metal atoms that are characterized by a diffuse unpaired s electron, and this gives a rough explanation of the smaller adhesion energies of Cu, Ag, and Au with respect to other transition metal atoms such as Pd or Ni.[67] It is still under debate whether chemical bonding plays a significant role in the adhesion of the coinage metals; further studies need to be carried out to clarify this point.

I.B. Dimers. The formation of a dimer can be viewed as the first step in the process of the growth of metal clusters on the oxide surface. The unit cell was chosen, consisting of a three-layer MgO (each layer containing nine O atoms and nine Mg atoms) and two metal atoms. Two possible sites of absorption on the regular surface have been considered

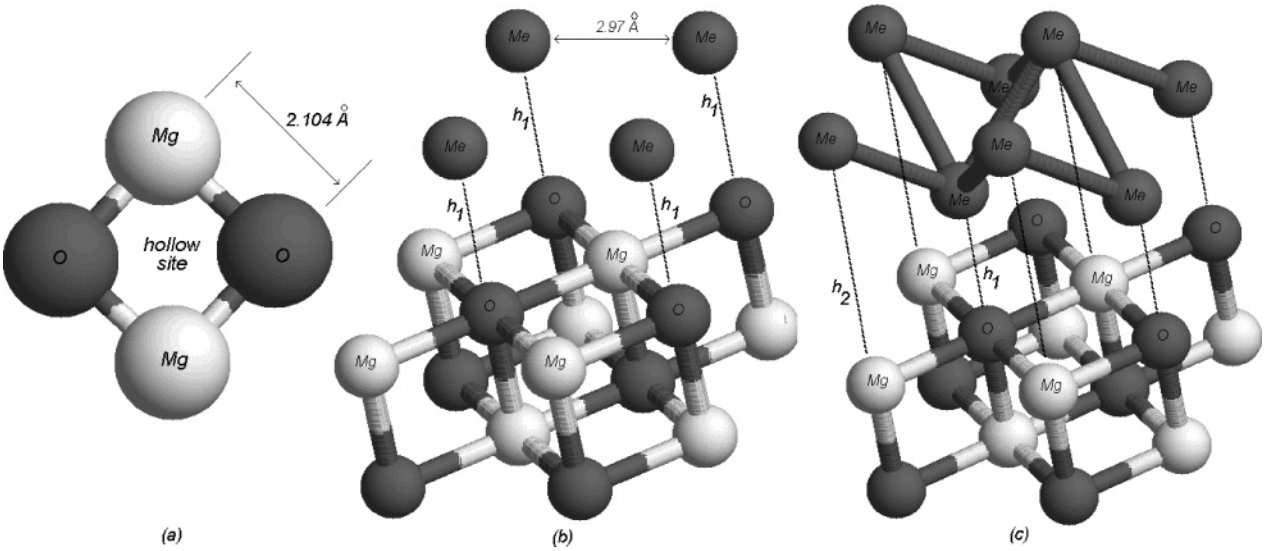

Figure 1. (a) Unit cell for a monolayer MgO slab. (b) One ML metal slab geometry absorption. (c) Two ML metal slab geometry absorption.

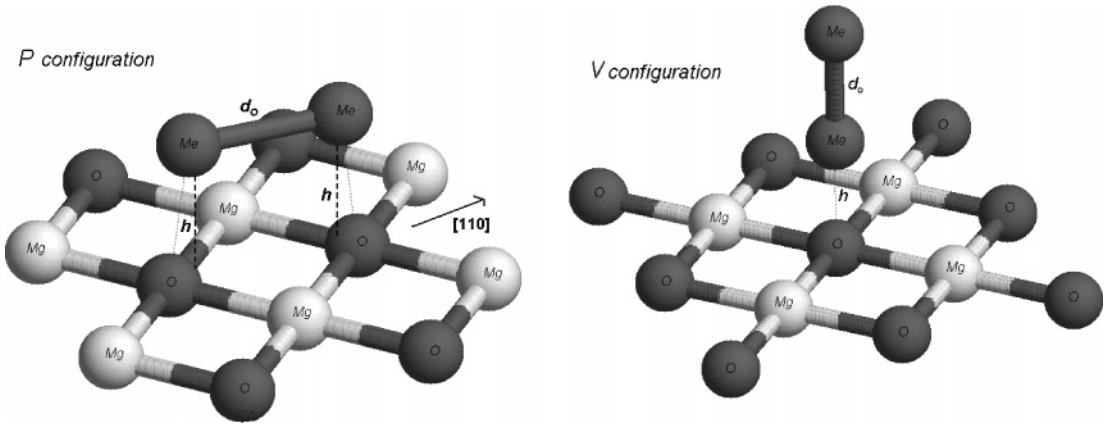

Figure 2. Dimer configurations on the regular MgO(100) surface.

Table 1. Interaction Energies and Distances Characterizing the Isolated Atom Absorption on the Regular MgO(100) Surface

adatoms		O site	Mg site	hollow site
Cu	E_{adh} (eV)	0.76	0.26	0.43
	d_o (Å)	2.1	2.8	2.3
Ag	E_{adh} (eV)	0.40	0.22	0.32
	d_o (Å)	2.5	2.9	2.6
Au	E_{adh} (eV)	0.87	0.49	0.67
	d_o (Å)	2.3	2.7	2.4

Table 2. (A) Characteristics of the Coinage Metal Dimers in the Gas Phase and (B) Geometric Parameters Characterizing the Geometric Configurations Shown in Figure 2

A. Characteristics of the Coinage Metal Dimers

	Cu_2	Ag_2	Au_2
binding energy (eV)	2.09	1.72	2.33
equilibrium bond length (Å)	2.25	2.59	2.52

B. Geometric Parameters

		d_0 (Å)	h (Å)	E_{int} (eV)	E_{adh} (eV)	ΔE_{met} (eV)
Cu_2	P	2.31	2.49	2.96	0.89	0.02
	V	2.26	2.16	3.24	1.15	0.00
Ag_2	P	2.61	2.79	2.18	0.46	0.00
	V	2.59	2.41	2.39	0.68	0.01
Au_2	P	2.56	2.63	2.92	0.61	0.02
	V	2.53	2.31	3.75	1.42	0.00

as interesting for a study of growth and diffusion (see Figure 2). The optimized values for the geometric parameters and the interaction energies are reported in Table 2b, while in Table 2a, the properties of the gas-phase dimers are reported.

The coinage metal dimers exhibit a similar behavior when absorbed on the regular surface. The values of the adhesion energy follow the same order characterizing the isolated adatoms: Au > Cu > Ag. The most stable geometry corresponds to the V configuration, in which the dimer is perpendicular to the surface atop the O^{2-} ion site. For Cu, this is in agreement with the results of refs 29−32, although we do not find any tilt angle with respect to the surface because we perform a symmetry-constrained relaxation along the surface normal direction. Although only one metal atom interacts with the surface, the adhesion energy of the dimer is *larger* than the value characterizing the isolated adatom.

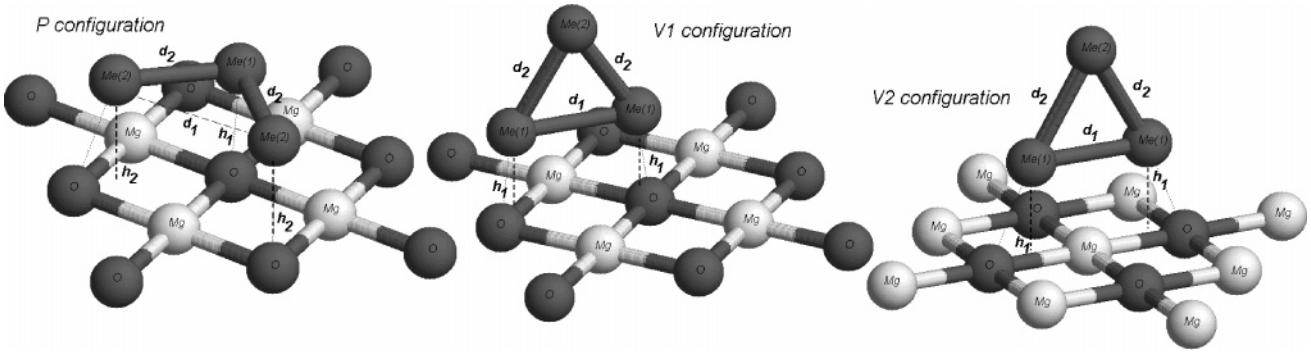

Figure 3. Trimer configurations on the regular surface. The last configuration on the right corresponds to the relaxation of the Au trimer on the F_s vacancy.

This result can be viewed as a first manifestation of the tendency of a vertical 3D growth of the coinage metal deposition on the oxide surface[29] and can be explained in terms of a stabilizing interaction between the dimer electron density and the field of the ionic surface.[103] In other words, the presence of metal atoms *above* those directly interacting with the surface *increases* the adhesion energy. This is what we call a "metal-on-top" stabilization mechanism. In the P configuration, the metal atoms can interact with two different O^{2-} ions, but the interaction energy is reduced because of the work needed to stretch the intermetal distance from the equilibrium value characterizing the isolated molecule. As a consequence, an almost identical intermetal distance is retained in all configurations considered and very small values of ΔE_{met} are observed.

To describe the diffusion process of the dimers on the surface, a leapfrog mechanism has been proposed for Cu, passing through the P configuration[29] with an activation energy barrier of 0.04 eV, although we find a larger energy difference between the V and P configurations.

It is interesting to note that, at variance with the coinage metal dimers, the most stable configuration for Pd_2 is the P one,[96] with the dimer parallel to the surface in a quasi-epitaxial geometry. This is due to a weaker metallic bond (especially noteworthy for the Pd_2 dimer) and a metal-on-top effect (probably because of a weaker polarizability of the d electrons with respect to the outer s electron).

I.C. Trimers. The chosen configurations are depicted in Figure 3. The unit cell was chosen, consisting of a three-layer MgO (each layer containing nine O atoms and nine Mg atoms) and three metal atoms. The values of the geometric parameters and of the interaction energies for each configuration are reported in Table 3b.

The trimers of the coinage metals are characterized by an s^3 electronic configuration, which produces a Jahn−Teller distortion and a consequent symmetry breaking from an equilateral triangle to an isosceles triangle. Looking at the optimized geometries of the three metals, we note that the distance between the central atom and the two lateral atoms is optimized at almost the equilibrium value of the gas-phase structure (reported in Table 3a), while the distance between the two lateral atoms is optimized in order to achieve the best interaction with the surface. Because of the Jahn−Teller effect, stretching the distance of the two lateral atoms does not imply any appreciable destabilization of the metal cluster.

Table 3. (A) Binding Energies and Geometric Parameters of the Coinage Metal Trimers in the Gas Phase and (B) Values of the Geometric Parameters Reported in Figure 4

A. Binding Energies and Geometric Parameters

	Cu_3	Ag_3	Au_3
binding energy (eV)	3.40	2.59	3.60
bond length d_1 (Å)	2.61	3.09	2.90
bond length d_2 (Å)	2.32	2.66	2.61

B. Values of Geometric Parameters

		d_1 (Å)	d_2 (Å)	h_1 (Å)	h_2 (Å)	E_{int} (eV)	E_{adh} (eV)	ΔE_{met} (eV)
	P	3.77	2.37	2.25	2.17	4.50	1.29	0.19
Cu_3	V1	2.61	2.33	2.10		5.00	1.60	0.00
	V2	3.50	2.36	2.06.		4.85	1.62	0.17
	P	4.33	2.69	2.73	2.67	3.27	0.72	0.04
Ag_3	V1	3.08	2.66	2.43		3.51	0.92	0.00
	V2	4.00	2.66	2.51		3.45	0.90	0.04
	P							
Au_3	V1	2.91	2.62	2.32		5.15	1.56	0.00
	V2	3.38	2.60	2.29		5.28	1.76	0.08

We refer to this behavior as *fluxional* (see the small values of ΔE_{met}). The larger values of ΔE_{met} for Cu are due to its shorter intermetal distances, which have to be stretched more to achieve a good interaction with the stabilizing sites of the surface.

As for the dimers, the preferred configurations of the trimers are the ones in which the cluster is perpendicular to the surface,[29] because of the metal-on-top stabilization mechanism. It can be noted that in the Au case, this effect is so strong that the P configuration relaxes toward the V2 configuration. These results are in fair agreement with those of ref 29 and suggest that the diffusion of the coinage trimers can take place through movements of "twisting" between the V1 and the V2 configurations, with low activation energy barriers especially for Ag and Au (slightly larger for Cu).

I.D. Extended Deposition. We built a unit cell assuming a pseudomorphic growth of the metal slab upon the oxide surface,[102,103] that is, positioning each metal atom above an O^{2-} (see Figure 1b), a Mg^{2+}, or a hollow site. Such a configuration corresponds to the growth of the (100) metal surface above the (100) oxide surface. Although the surface energy of the (100) surface is larger than the surface energy of the (111) surface for all the metals considered, the simplest metal configuration compatible with the symmetry of the

Table 4. Results for the Absorption of One and Two MLs on the Regular Surface[a]

		one ML			two ML		
		O site	Mg site	hollow site	O site	Mg site	hollow site
Cu	E_{int} (eV)	1.95	1.67	1.75	2.75	2.52	2.57
	E_{adh} (eV)	0.32	0.045	0.13	0.50	0.041	0.15
	h_1 (Å)	2.3	3.4	2.7	2.2	3.4	2.6
	h_2 (Å)				3.4	4.6	3.8
Ag	E_{int} (eV)	1.80	1.67	1.72	2.12	2.03	2.05
	E_{adh} (eV)	0.16	0.036	0.083	0.24	0.066	0.10
	h_1 (Å)	2.8	3.4	3.0	2.6	3.9	2.9
	h_2 (Å)				4.6	5.9	4.9
Au	E_{int} (eV)	2.26	2.20	2.24	2.66	2.59	2.62
	E_{adh} (eV)	0.15	0.095	0.13	0.22	0.084	0.15
	h_1 (Å)	2.9	3.1	2.9	2.8	3.3	2.9
	h_2 (Å)				4.8	5.3	4.9

[a] h_1 and h_2 respectively correspond to the heights of the first and the second metal layers on the MgO surface.

oxide cell is the one adopted here. The strict constraint of this assumption is that the first neighbor distance between the metal atoms of the slab is fixed at the value 2.975 Å. The chosen cell consists of three MgO layers, each containing only two Mg atoms, two O atoms, and two (four) metal atoms in the case of one (two) ML absorption (a five-layer slab model gave essentially identical results). In the two ML case, the atoms of the second metal slab were positioned in the interstitial sites of the first slab in such a way as to build the *fcc* structure of the bulk metals.

One ML. The results of one ML absorption are reported in Table 4, in which all energies are per atom. The values of ΔE_{met} are not reported because we did not perform a calculation by relaxing the reticular lattice parameter of the isolated metal ML.

From the results, which are in agreement with those reported in ref 103, we can derive the following observations:

(1) The order of stability of the three possible sites of absorption is the same as that found for the isolated atoms; the best configuration corresponds to all metal atoms on top of the O atoms on the surface.

(2) For all of the three system considered, there is a decrease of the adhesion energy per atom with respect to the case of the isolated atoms and a corresponding increase of the equilibrium distance between the metallic slab and the oxide surface.

(3) The absolute value of the adhesion energy decrease is remarkably large for Au on top of the O atoms; as a consequence, the stability order among the three metals is no longer Au > Cu > Ag (as for the isolated adatoms) but Cu > Ag ≈ Au.

To explain this behavior, two physical factors have to be taken into account: (1) the mismatch between the metal lattice constant and the reticular constant characterizing the pseudomorphic growth and (2) the strength of the metallic bond. The weak adhesion of the Au ML to the surface is due to the small mismatch between the reticular constant of bulk gold (2.885 Å) and the lattice parameter imposed by the pseudomorphic growth (2.975 Å), which implies a strong metal bond and, thus, a decreased interaction energy with the surface. Cu is characterized by a metal bond of strength comparable to Au, but the small value of the reticular constant of bulk copper corresponds to a large mismatch (about 16%) between the metal and the oxide lattice. The adhesion with the surface, thus, overcomes the metal binding energy.

Note, however, that these considerations neglect the change in the nearest-neighbor distances due to reduced coordination (from 12 to 4) in the one ML case. This determines a contraction of the lattice parameter,[57] consequently increasing the mismatch with the reticular constant of the oxide.

Two ML. The results for these systems are summarized in Table 4. Note that the adhesion energies are calculated normalizing the total interaction energy to the number of atoms in contact with the oxide surface (as we did in the case of the monolayer). [This is not a universally accepted convention, and some authors prefer to normalize the adhesion energy to the number of total atoms (considering those involved in the direct interaction with the surface and also the atoms in the second layer).] The general behavior is very similar to the one ML case: the order of stability among the three metals is Cu > Ag ≈ Au, and so forth. In passing from one to two ML deposition, however, one observes an increase in the adhesion energy (in a remarkable way, for the absorption atop the O^{2-} site). This increase in the adhesion energy has already been observed for Cu and Ag extended deposition[103] and explained in terms of the enhanced electrostatic polarization of the metallic electronic cloud in the surface field of the oxide, what we call a "metal-on-top" effect, in excellent agreement with the stabilization of the upright configurations reported in Sections I.B and I.C for the dimers and trimers. This happens despite the fact that the increase in the coordination number of the metal (from 4−8) increases its lattice constant, thus decreasing the mismatch with the lattice constant of the oxide and, consequently, enhancing the metallic bond in the slab.

We conclude this section by stressing that, when treating isolated atoms, among the coinage, we can distinguish between Cu and Au from one side and Ag on the other: Cu and Au are more strongly bound to the surface, while the interaction of Ag is much weaker. On the contrary, when passing to the extended deposition of one and two MLs, we observe a leveling of the adhesion energies among the three metals, with a pronounced resemblance between Ag and Au with respect to Cu.

II. Interaction of Coinage Metal Clusters with the an F_s Defect of the MgO(100) Surface. The F_s defect is formed when a neutral O atom leaves the MgO(100) surface but the two electrons carrying the negative charge of the O atom are kept in the vacancy. As the F_s vacancy constitutes a good candidate as a center of nucleation for the absorption of several transition metals on the oxide surface, this kind of defect has been extensively studied both experimentally and theoretically in recent years.

We considered the same unit cells used for the absorption on the regular surface: a three-layer MgO, each layer containing four or nine Mg and O atoms, depending on the size of the adsorbed metal cluster. Selected calculations using larger cells have also been performed, producing essentially comparable results.

Table 5. Adatoms Absorbed Atop the F_s Vacancy

adatoms	Cu	Ag	Au
$E_{adh} = E_{int}$ (eV)	1.76	1.59	3.04
h_o (Å)	1.80	2.00	1.81

Table 6. Dimer Geometries and Interaction Energies of the Coinage Dimers on the F_s Defect

		P	V		P	V
Cu_2	d_0 (Å)	2.33	2.34	E_{int} (eV)	4.13	4.16
	h_1 (Å)	1.55	1.68	E_{adh} (eV)	2.05	2.09
	h_2 (Å)	2.86	4.02	ΔE_{met} (eV)	0.01	0.02
Ag_2	d_0 (Å)	2.65	2.64	E_{int} (eV)	3.59	3.62
	h_1 (Å)	1.80	1.82	E_{adh} (eV)	1.89	1.92
	h_2 (Å)	3.91	4.46	ΔE_{met} (eV)	0.01	0.01
Au_2	d_0 (Å)	2.59	2.59	E_{int} (eV)		6.05
	h_1 (Å)	1.60	1.60	E_{adh} (eV)		3.75
	h_2 (Å)	4.19	4.19	ΔE_{met} (eV)		0.03

As anticipated before, the reconstruction of the MgO lattice around the F_s vacancy is negligible both in the absence and in the presence of metal absorption, in agreement with previous studies.[67,70] For this reason, we did not perform any relaxation of the MgO surface ($\Delta E_{MgO} = 0$).

II.A. Isolated Adatoms. The single atoms are trapped atop the F_s center. The values of the interaction energy and of the equilibrium distance are reported in Table 5 and are in fair agreement with the results reported in ref 67.

The order among the three metals is same as that for the adsorption on the regular surface. The atoms can get closer to the vacancy on the surface because of the decrease of the Pauli repulsion consequent to the removal of the O atom, thus experiencing a stronger electric field, with a consequent increase of the polarization interaction. The relative increase of the interaction energy is larger in the cases of Ag and Au with respect to Cu, probably because of chemical bond effects.

II.B. Dimers. We considered the same configurations used for the absorption on the regular surface (see Figure 2). In Table 6, the geometric parameters and the energies for each configuration are reported.

The results for the P configuration of Au_2 is not reported because it relaxes toward the perpendicular configuration atop the vacancy (V configuration).

As for the perfect surface, the intermetal distances are only slightly elongated with respect to the equilibrium gas-phase values; the distortion energies are consequently very small. Also, the differences in adhesion and interaction energies between the P and V configurations are very small; this can be explained by noting that the P configuration is remarkably tilted with respect to the surface, so the dimers in the two configurations probably experience a similar field.

The interaction mechanism is the same as that for the adsorption of a single atom on the F_s center. Only, the decrease in equilibrium distances and, thus, the stabilizing effect are still more pronounced, as a result of the metal-on-top mechanism.

II.C. Trimers. We chose two configurations: one is similar to V1 from Figure 3, in which the F_s vacancy is under a lateral metal atom, and the other one is a linear epitaxial configuration, in which the F_s vacancy is under one of the lateral atoms. The geometric parameters and the energies characterizing the absorption of the coinage metal trimers on the F_s vacancy are reported in Tables 7 and 8, from which it can be seen that an appreciable rearrangement of the metal atoms not directly bound to the defect occurs. The dominant contribution to the adhesion energy is given by the interaction of the metal atom atop the defect. As a result of the fluxionality of the trimers and the interplay between the metal-on-top effect and the direct metal−surface interaction, there exists a large set of different configurations very close in energy, among which we selected two representative ones, without being certain to have singled out the absolute energy minimum. As before, the energy differences are slightly larger for Cu, because of its reduced fluxionality. The order of stability among the three coinage metals is the same as that found in the previous sections. The adhesion energies for all three metals are still larger than for the dimers, as fluxionality allows the trimers to deform in such a way as to better interact with the surface and exploit the metal-on-top effect or the direct metal−surface interaction.

Table 7. Geometric Parameters for the Coinage Trimers Absorbed on the F_s Vacancy[a]

		d_{1-2} (Å)	d_{2-3} (Å)	d_{1-3} (Å)	h_1 (Å)	h_2 (Å)	h_3 (Å)
Cu_3	V1	2.58	2.36	2.40	1.68	2.17	3.90
	L1	2.47	2.37	4.80	1.91	2.48	2.43
Ag_3	V1	2.97	2.73	2.70	1.80	2.67	4.40
	L1	2.73	2.71	5.30	1.92	3.04	2.92
Au_3	V1	2.80	2.69	2.69	1.57	2.85	4.25
	L1	2.67	2.62	4.68	1.66	3.37	2.65

[a] The atom labeled 1 is the one absorbed atop the vacancy.

Table 8. Energies Involved in the Trimer Absorption on the F_s Vacancy

		E_{int} (eV)	E_{adh} (eV)	ΔE_{met} (eV)
Cu3	V1	6.12	2.75	0.03
	L1	5.58	2.48	0.31
Ag3	V1	4.96	2.39	0.02
	L1	4.78	2.25	0.07
Au3	V1	7.80	4.24	0.04
	L1	7.70	4.09	0.01

The main conclusion that we can extract from the results of the absorption of atoms, dimers, and trimers on the oxygen vacancy is that the defect acts as a strong trapping center for all the coinage metals. The differences in adhesion between several configurations are small with respect to the absolute values of the absorption energies found in the calculations. Every possible mechanism of diffusion of small clusters from the site of the vacancy to the neighboring regular sites is strongly disfavored; the more it is disfavored, the larger the metal cluster.

II.D. Extended Depositions. One ML. The mean values of the adhesion and adsorption energies are evaluated by calculating the total absolute value of the respective energies and dividing by the number of the atoms in contact with the surface (four both for one and two MLs). The word "mean" refers to the fact that the single atoms experience a different

Table 9. One and Two MLs Absorbed on the F_s Vacancy

	one ML			two ML		
	Cu	Ag	Au	Cu	Ag	Au
$\langle E_{int} \rangle$ (eV)	2.14	1.99	2.72	2.84	2.25	2.85
$\langle E_{adh} \rangle$ (eV)	0.54	0.41	0.84	0.68	0.47	0.79
$\langle \Delta E_{met} \rangle$ (eV)	0.03	0.06	0.20	0.01	0.01	0.09
h_1 (Å)[a]	1.79	2.00	1.71	1.83	2.31	1.80
h_2 (Å)[b]	2.41	2.84	2.90	2.17	2.74	2.69
h_3 (Å)[c]	2.54	2.96	2.99	2.18	2.77	2.73

[a] Distance of the metal atom atop the vacancy. [b] Distance of the metal atom atop an O ion at 2.97 Å away from the vacancy. [c] Distance of the metal atom atop an O ion at 4.21 Å away from the vacancy.

Table 10. Coinage Dimers on the Double Vacancy

	Cu_2	Ag_2	Au_2		Cu_2	Ag_2	Au_2
d_o (Å)	2.43	2.68	2.69	E_{int} (eV)	5.51	4.23	5.21
h_1 (Å)[a]	0.191	0.525	0.467	E_{adh} (eV)	4.56	3.21	3.89
h_2 (Å)[b]	1.59	2.10	2.04	ΔE_{met} (eV)	0.11	0.02	0.12
r_{1-Mg} (Å)	0.089	0.276	0.370	ΔE_{MgO} (eV)	1.03	0.68	0.89
r_{2-O} (Å)	0.028	0.336	0.442	ΔE_{relax} (eV)	0.86	0.60	0.73

[a] Height of the atom atop the Mg^{2+} empty site. [b] Height of the atom atop the O^{2-} empty site.

interaction with the surface. The sites of absorption are four: one atop the vacancy, two on regular O^{2-} ions at a distance of 2.97 Å from the defect, and one on a regular O^{2-} at a distance 4.21 Å from the defect. The results are reported in Table 9. The values reported as $\langle \Delta E_{met} \rangle$ correspond to the energy increase due to the corrugation of the metal slab.

The final relaxed topology of the metallic slab is characterized by a corrugation due to the different heights of the metal atoms upon the four different sites of the surface. The atom directly atop the vacancy lies almost at the equilibrium height characterizing the isolated adatom, which suggests that this atom is practically not involved in the metallic bond with the other metal atoms. By using the data of Table 4, we can give an estimate of the interaction energy of the lower metal atom with the vacancy: supposing that the three metal atoms on the regular sites interact with the surface with the same amount of adhesion energy characterizing the one ML on the regular surface, we get

- Cu: 1.44 eV (real value of the adatom: 1.76 eV)
- Ag: 1.28 eV (real value of the adatom: 1.59 eV)
- Au: 3.02 eV (real value of the adatom: 3.04 eV)

In the one ML system, the interaction of the lower atom with the vacancy is decreased by about 20% in the cases of Cu and Ag and only less than 1% in the case of Au.

Two ML. When studying the absorption of a second monolayer absorbed on the first one, we do not find any corrugation of the second metal layer. The results are reported in Table 9.

It can be noted that for Cu and Ag, we observe an increase of the adhesion energy and a corresponding decrease of the distance of the metal atoms on the regular sites from the surface. On the contrary, Au exhibits a decrease of the adhesion energy; the stabilization due to the metal-on-top effect does not manage to compensate for the loss of the metal bond energy due to the corrugation of the first layer.

III. Interaction of Coinage Metal Clusters with the a Double Vacancy of the MgO(100) Surface. Another surface defect that has attracted considerable interest in recent years is the double vacancy.[100] This is a neutral defect and corresponds to the removal of an MgO dimer in the 100 direction of the regular oxide terrace. Its surface concentration is estimated to be rather high.[7,72] The difference with respect to the F_s defect, which, as we will see, has important consequences in view of the nucleation process, is that the removal of an MgO dimer induces an appreciable modification in the structure of the oxide slab. In fact, allowing relaxation of the defected surface results in an increase of the dimensions of the cavity with a corresponding stabilization energy of about 2.90 eV. The distances between the prospicient atoms at the border of the cavity increase by up to 10% with respect to the nonrelaxed values (see Figure 4a, where some characteristic distances between the borders of the cavity are reported).

As anticipated above, we always relaxed all the geometric parameters upon absorption. The unit cell of the MgO slab is made of three layers containing a total of 52 atoms. This is the largest unit cell we have considered, and this, together with the need of optimizing the degrees of freedom also corresponding to the MgO surface, means that the calculations involving the divacancy are the most computationally intensive.

III.A. Isolated Atoms. The results of the absorption of single coinage metal atoms on the double vacancy are reported in Table 11. In the table, E_{int}, E_{adh}, ΔE_{MgO} are the quantities defined at the beginning of Section 3; ΔE_{relax} is a new quantity defined as the energy gain obtained by performing a relaxation of the cluster coordinates, keeping the coordinates of the lattice frozen in the position characterizing the relaxed isolated oxide, and it is useful in checking the validity of the quadratic expansion of the interaction energy (see below).

From the analysis of the data from Table 11, two common features can be derived: (1) All the metals adsorb near the site left empty by the removal of the Mg atom; all the adsorbed atoms go deeply into the cavity reaching almost the same height as the Mg and O atoms of the surface oxide layer. (2) The interaction energies with the divacancy are of the same order of magnitude as the energies characterizing the interaction with the F_s defect, suggesting that this defect is another good candidate as a nucleation site on the MgO-(100) terrace.[100]

Some quantitative differences can be evinced through a more detailed analysis: Cu has the smallest size and, thus, it gets closer than Ag or Au to the empty site of the Mg^{2+} ion. In such a way, it can interact with the O^{2-} ion beneath it and also with the other three O^{2-} ions at the borders of the vacancy. On the other hand, Ag and Au are too big to get close to the empty site of the Mg^{2+} ion and move toward the center of the vacancy, still keeping an appreciable interaction with the four O^{2-} surrounding ions. These considerations are confirmed by the amount of the MgO lattice "back relaxation", that is, the distortion energy of the lattice in the configuration optimally interacting with the metal atom with respect to the isolated relaxed defect,

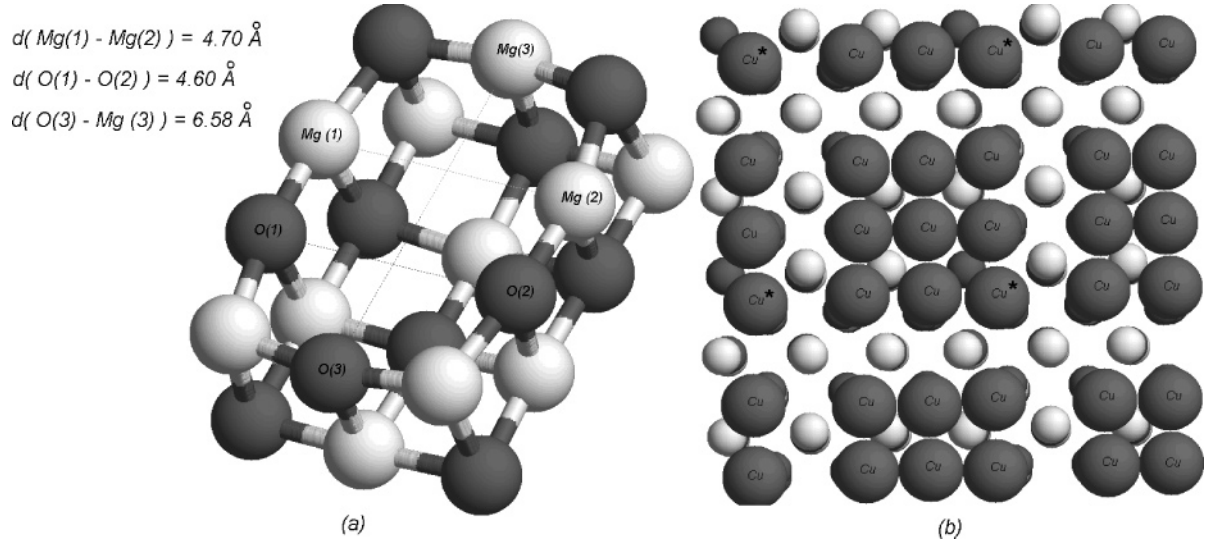

Figure 4. (a) Relaxed geometry of the oxide surface around the divacancy. (b) Cu_9 island formation; the Cu* atoms are the ones absorbed upon the vacancy.

Table 11. Interaction Energies and Characteristic Distances of the Isolated Adatoms on the Double Vacancy

adatoms	Cu	Ag	Au
E_{int} (eV)	2.83	1.95	2.34
E_{adh} (eV)	3.94	2.47	2.90
ΔE_{MgO} (eV)	1.11	0.522	0.568
ΔE_{relax} (eV)	0.778	0.454	0.481
h_o (Å)	0.189	0.547	0.501
distance from Mg site (Å)	0.176	0.585	0.781

expressed as ΔE_{MgO} in Table 11. In the case of Cu, the relaxed oxide lattice *closes* around the metal atom (ΔE_{MgO} has a value of 1.11 eV) much more than for Ag and Au. Finally, it can be noted that the values of ΔE_{relax} are roughly proportional to the values of ΔE_{MgO}, in agreement with a quadratic expansion of the interaction energy (see, e.g., ref 116).

III.B. Dimers. Whatever the starting configuration, all the coinage metal dimers relaxed to a configuration with the two atoms of the molecule atop the two empty sites of the vacancy. This behavior is analogous to the absorption of the Pd dimer on the double vacancy.[100] The remarkable stability of this configuration is due to the fact that the two atoms can interact with the three O^{2-} ions and the three Mg^{2+} ions at the border of the cavity; both atoms of the metal cluster can get close to the surface thanks to the big dimensions of the cavity. Our results are reported in Table 10.

The order of stability among the coinage metals is the same as that for the absorption of the single adatom; furthermore, also in this case, the smaller dimensions of the Cu dimer favor an enhanced backward movement of the oxide lattice around the cluster absorbed (see the values of ΔE_{MgO}). Again, the gain in interaction energy due to the relaxation of the oxide lattice (i.e., the values of ΔE_{relax}) are roughly proportional to ΔE_{MgO}, in fair agreement with the quadratic expansion theorem, showing that the system is roughly in the linear regime. This is further confirmed by the fact that the value of ΔE_{relax} is approximately proportional to the corresponding adhesion energy (ΔE_{adh}).

Table 12. Coinage Trimer Geometries on the Double Vacancy

	Cu_3		Ag_3		Au_3	
	A	B	A	B	A	B
d_{1-2} (Å)	2.49	2.44	2.68	2.70	2.63	2.64
d_{2-3} (Å)	2.47	2.61	2.76	2.82	2.65	2.61
d_{1-3} (Å)	2.38	2.39	2.80	2.79	2.81	2.91
h_1 (Å)[a]	0.217	0.255	0.789	0.808	1.13	1.15
h_2 (Å)[b]	1.56	1.67	2.17	2.17	1.82	1.84
h_3 (Å)	2.68	2.05	3.55	2.92	3.73	3.10

[a] Height of the atom atop the Mg^{2+} empty site. [b] Height of the atom atop the O^{2-} empty site

Table 13. Energies for the Trimers on the Double Vacancy

	Cu_3		Ag_3		Au_3	
	A	B	A	B	A	B
E_{int} (eV)	6.90	7.09	5.19	5.20	6.74	6.82
E_{adh} (eV)	4.65	5.00	3.23	3.28	4.11	4.26
ΔE_{met} (eV)	0.06	0.07	0.03	0.02	0.01	0.005
ΔE_{MgO} (eV)	1.09	1.24	0.60	0.65	0.96	1.03

III.C. Trimers. The geometries we considered are with two metal atoms on top of the two sites of the vacancy and the third metal atom either atop the other two (A), not in direct contact with the surface, or atop the O^{2-}(2) ion at the border of the cavity (B) (see Figure 4a for the nomenclature of the surface sites). The results of the calculations are reported in Tables 12 and 13.

The results for the three metals do not qualitatively differ very much: the two selected configurations are characterized by very similar values of the absorption energy, the distortion energies of the metallic clusters are quite small, and among the three coinage metals, the largest values are observed in the case of Cu, in agreement with the results of Sections I.C and II.C. As in the case of the interactions of the single atoms and dimers, the values of the distortion energy of the surface lattice are largest in the case of the absorption of Cu clusters

Table 14. One and Two MLs Absorbed on the Double Vacancy

	1 ML			2 ML		
	Cu	Ag	Au	Cu	Ag	Au
$\langle E_{int} \rangle$ (eV)	2.19	1.81	2.31	2.85	2.18	2.73
$\langle E_{adh} \rangle$ (eV)	0.47	0.25	0.31	0.78	0.32	0.50
$\langle \Delta E_{met} \rangle$ (eV)	−0.17	0.05	0.02	−0.02	−0.03	0.02
ΔE_{MgO} (eV)	0.70	0.29	0.67	1.37	0.67	1.00

[a] Distance of the metal atom atop the vacancy. [b] Distance of the metal atom atop an O ion at 2.97 Å away from the vacancy. [c] Distance of the metal atom atop an O ion at 4.21 Å away from the vacancy.

(because of the smaller dimensions of the Cu atom) and smallest in the case of Ag.

III.D. Extended Deposition. These results are reported in Table 14. The study of one (two) ML absorption above the double-vacancy defected MgO surface involves a heavy calculation implying the full relaxation of all the 61 (70) atoms per unit cell. For all three metals considered, a spin-restricted ground state was found. The chosen geometry is a pseudomorphic one with each metal atom atop a different O^{2-} ion of the surface layer. The particularity of this configuration is that one metal atom is put on top of the site of the vacancy with the weaker interaction (the empty O site).

The results of the calculations are discussed separately for the three coinage metals because of their peculiar behavior. Starting with Ag, for the which the discussion is simpler, we note that Ag is characterized by a good match between the lattice constant of the metallic layer and that of the oxide support. Moreover, Ag has a weaker interaction energy with the surface (both regular and defected) and a weaker metallic bond with respect to Au and Cu. The small value of ΔE_{MgO} (only 0.29 eV for one ML) and the fact that the metal atoms essentially maintain their starting positions suggest that the layer does not interact very much, even with the defected surface. In particular, the Ag atom atop the vacancy relaxes by simply decreasing its distance from the surface. The adhesion energy is quite low: 2.25 eV for nine atoms. If we take a value of 0.16 eV as the interaction energy of the eight atoms on the regular sites (the value characterizing the interaction with the regular surface), we obtain by difference that the atom atop the defect contributes about 0.9−1.0 eV, a value appreciably smaller than that for the absorption of the single atom on the divacancy (see Table 11).

Au, too, is characterized by a good match between the lattice constants of the metal and that of the oxide. However, Au interacts more strongly than Ag with the regular and defected surface sites of the surface and, at the same time, has a stronger metallic bond. The Au monolayer, thus, presents a more pronounced corrugation; in particular, the atom atop the empty O site remarkably decreases its distance from the surface (with a consequent weakening of its metal bonding), while the three Au atoms at the border of the vacancy move slightly inward. What we observe is a segregation of the metal slab with the formation of islands of nine atoms with the divacancy placed at one edge of the square (see Figure 4b for the case of Cu, in which this effect is even more pronounced). The stronger interaction with the surface is reflected in the larger value of the lattice distortion energy with respect to the Ag case.

The Cu monolayer exhibits the same behavior encountered in the Au case but in a more pronounced way. The larger mismatch between the Cu lattice constant and the surface lattice parameter and the stronger interaction of the Cu atom with the divacancy, in fact, determine a strong segregation of the metal slab with the formation of nine-atom islands (see Figure 4b). From the data of ΔE_{met} in Table 14, we observe that the formation of islands is accompanied by a strengthening of the metallic bond with respect to the pseudomorphic configuration. Segregation is also expected to occur in the absence of the divacancy defect, but it is significant that the defect places itself at a border of the metal islands; this suggests a peripheral growth of the metal cluster with respect to the double vacancy (at variance with the F_s center case, in which the cluster is expected to grow all around the defect).

The absorption of the second metal layer above the first one determines an increase of the values of ΔE_{MgO} and E_{adh} for all the three coinage metals, essentially because of the metal-on-top mechanism. In the case of Ag, the deposition of the second layer does not affect the geometry of the metal slab and the increase in adhesion energy is on the same order of magnitude as in the case of absorption on the regular surface and on the F_s defect. In the case of Cu and Au, the presence of the second metal layer above the first one prevents the segregation observed in the case of the single monolayer, thus increasing the direct interaction of the first metal slab with the surface and the metal-on-top effect. The increase in adhesion energy is consequently larger than in the case of absorption on the regular terrace and that on the single vacancy.

4. Conclusions

The results of a systematic study of the interaction of small coinage metal clusters (M_n, $n = 1-3$) and extended deposition (one and two ML) with the regular and locally defected (F_s center and divacancy) neutral MgO(100) surface are presented. These results can be summarized as follows, underlining analogies and differences between the three coinage metals.

In agreement with previous work,[65−67] the most stable site of nucleation on the regular surface for all the isolated adatoms is the O^{2-} ion. The interaction energy is larger in the case of Cu and Au with respect to Ag. This order of interaction energies is found to hold for nearly all the systems considered. In the dimers, the metal chemical bond is stronger than the interaction with the surface and the "sticky" character of the metallic bond prevents the stretching of the metal−metal distance from the equilibrium value characterizing the isolated dimers. The most stable configuration is perpendicular to the surface. Despite the fact that only one atom interacts with the surface, the adhesion energy of the cluster is larger than that for the single adatom, which suggests that the presence of metal atoms *on-top* of those directly interacting with the surface *increases* the adhesion energy ("metal-on-top" stabilization mechanism). A peculiar characteristic of the coinage metal trimers is their fluxional

behavior, originating from the Jahn−Teller symmetry breaking due to the electronic configuration of these molecules. As in the case of the dimers, the configurations perpendicular to the surface are the most stable ones ("metal-on-top" stabilization mechanism). Nevertheless, thanks to their fluxionality, the trimers manage to optimize both the metallic bond and the adhesion with the surface in several different configurations. The consequently small energy differences between the corresponding local minima allow the diffusion of the clusters on the surface even at rather low temperatures. This is particularly true for Ag and Au, which are characterized by longer intermetal bond lengths with respect to Cu and a, thus, smaller mismatch with the oxide lattice parameter.

For the absorption of extended pseudomorphic deposition (one and two ML), Ag[83,103,104] and Au are characterized by a good match between the bulk metal lattice constant and the lattice constant of the oxide pattern. The strength of the metallic bond then determines a decrease of the adhesion energy with the surface in passing from small clusters to extended deposition, especially in the case of Au, for the which the metallic bond is stronger and "stickier".[57] Instead, the mismatch between the lattice parameters of the Cu overlayer and the surface determines a smaller decrease of the adhesion energy with the surface.[83,103,104] For all three coinage metals, the thickening of the metal slab from one to two MLs determines an increase of the adhesion energy per atom in agreement with the "metal-on-top" stabilization mechanism.

In the case of the F_s center and the double vacancy, it is found that these defects act as strong trapping centers for small clusters and strongly increase the adhesion of metal slabs to the surface in the case of extended deposition.[67,108] The main difference between the two defects is that the presence of the double vacancy induces a strong structural and energetic modification in the surrounding oxide lattice;[67] moreover, such a structural relaxation changes according to the extent of the metal deposition upon the surface. On the contrary, the presence of the single vacancy induces negligible structural and energetic modifications of the oxide lattice both in the absence and in the presence of the metal deposition.

In the case of the single vacancy, the metal atoms can get closer to the surface because of the decreased Pauli repulsion consequent to the removal of the O atom.[103] The adhesion energy is stronger for Au than for Cu and Ag; since the dimensions and the polarizability of the gold atom are similar to those of Ag, this suggests that chemical bonding effects are important for Au. The most stable configurations of dimers and trimers are, again, those in which the cluster is perpendicular to the surface, with one of the lower atoms directly atop the vacancy. In the case of extended deposition, the atom atop the vacancy is weakly involved in the metallic bond. In the case of the two ML absorption, we observe an increase of the adhesion energy in the case of Cu and Ag but not for Au, for which the distortion of the metal structure overwhelms the stabilization as a result of the thickening of the metal slab.

In the case of the double vacancy, the metal atoms are free to choose between the two possible sites of the vacancy (the empty Mg site or the empty O site). Ag and Au, which are bigger than Cu, move toward the center of the cavity in order to reduce the Pauli repulsion with the O^{2-} ions at the border. Cu, instead, absorbs near the empty Mg site and, consequently, interacts much more strongly with the surface. In the case of the dimers and trimers, two metal atoms occupy the two empty sites of the surface. In the case of extended deposition, the pseudomorphic growth is disfavored by the fact that the metal atom directly above the cavity is atop the O empty site. For Cu and Au, this, together with the mismatch between the Cu lattice parameter of the metal and that of the oxide, induces the formation of segregated metal islands with the cavity at one of the corners. This effect is decreased in the two ML case, in which the adhesion energy increases appreciably for all three coinage metals.

To briefly summarize, we find that coinage metals can easily diffuse on the perfect MgO(100) surface, with small clusters diffusing even faster than single atoms, to be strongly trapped at local defects, such as the F_s center and the divacancy, which can, thus, act as nucleation centers. The presence of metal atoms above those directly interacting with the surface increases the adhesion energy, according to a "metal-on-top" mechanism, for both perfect and defected oxide. A peculiar structural relaxation is found for the divacancy, which suggests a "peripheral" growth of the metal clusters.

Acknowledgment. We thank Gianfranco Pacchioni (Milano, Italy) and Riccardo Ferrando (Genova, Italy) for useful discussions. We acknowledge financial support from the Italian CNR for the project "(Supra-)Self-Assemblies of Transition Metal Nanoclusters" within the framework of the ESF EUROCORES SONS and from the European Community Sixth Framework Programme for the STREP project "Growth and Supra-Organization of Transition and Noble Metal Nanoclusters" (Contract NMP4-CT-2004-001594). A.F. acknowledges the Italian INSTM for a grant at the CINECA supercomputing center. (After the manuscript was submitted, we learned of a related work on Au small clusters absorbed on regular and defected MgO surfaces[117]).

Acknowledgment. This section tagged Supporting Information

Supporting Information Available: Additional data on configurations. This material is available free of charge via the Internet at http://pubs.acs.org.

References

(1) Aiken, J. D., III; Finke, R. G. *J. Mol. Catal. A* **1999**, *145*, 1−44.

(2) Jensen, P. *Rev. Mod. Phys*. **1999**, *71*, 1695−1735.

(3) Henry, C. R. *Surf. Sci*. **1998**, *31*, 235−325.

(4) Pileni, M.-P. *J. Phys. Chem. B* **2001**, *105*, 3358−3371.

(5) Henry, C. R.; Meunier, M. *Mater. Sci Eng*., A **1996**, *A217/218*, 239−243.

(6) Leroy, F.; Revenant, C.; Renaud, G.; Lazzari, R. *Appl. Surf. Sci.* **2004**, *238*, 233−237.

(7) Revenant, C.; Leroy, F.; Lazzari, R.; Renaud, G.; Henry, C. R. *Phys. Rev. B* **2004**, *69*, 035411.

(8) Renaud, G. *Surf. Sci. Rep*. **1998**, *32*, 1−90.

(9) Renaud, G. *Science* **2003**, *300*, 1416−1419.

(10) Thornton, G. *Science* **2003**, *300*, 1378−1379.

(11) Hansen, K. H.; Ferrero, S.; Henry, C. R. *Appl. Surf. Sci.* **2004**, *226*, 167−172.

(12) Becker, C.; Rosenhahn, A.; Wiltner, A.; Von Bergmann, K.; Schneider, J.; Pervan, P.; Milun, M.; Kralj, M.; Wandelt, K. *New J. Phys*. **2004**, *4*, 75.1−75.15.

(13) Degen, S.; Becker, C.; Wandelt, K. *Faraday Discuss*. **2004**, *125*, 343−356.

(14) Becker, C.; Von Bergmann, K.; Rosenhahn, A.; Schneider, J.; Wandelt, K. *Surf. Sci.* **2001**, *486*, L443−L448.

(15) Wiltner, A.; Rosenhahn, A.; Schneider, J.; Becker, C.; Pervan, P.; Milun, M.; Kralj, M.; Wandelt, K. *Thin Solid Films* **2001**, *400*, 71−75.

(16) Xu, C.; Oh, W. S.; Liu, G.; Kim, D. Y.; Goodman, D. W. *J. Vac. Sci. Technol., A* **1997**, *15*, 1261−1268.

(17) Yoon, B.; Luedtke, W. D.; Gao, J.; Landman, U. *J. Phys. Chem. B* **2003**, *107*, 5882−5891.

(18) Bréchignac, C.; Cahuzac, P.; Carlier, F.; Colliex, C.; Leroux, J.; Masson, A.; Yoon, B.; Landman, U. *Phys. Rev. Lett.* **2002**, *88*, 196103.

(19) Moseler, M.; Hakkinen, H.; Landman, U. *Phys. Rev. Lett*. **2002**, *89*, 176103.

(20) Campbell, C. T.; Starr, D. *J. Am. Chem. Soc*. **2002**, *124*, 9212−9218.

(21) Kim, Y. D.; Stultz, J.; Wei, T.; Goodman, D. W. *J. Phys. Chem. B* **2002**, *106*, 6827−6830.

(22) Larsen, J. H.; Ranney, J. T.; Starr, D. E.; Musgrove, J. E.; Campbell, C. T. *Phys. Rev. B* **2001**, *63*, 195410.

(23) Suzuki, T.; Hishita, S.; Oyoshi, K.; Souda, R. *Surf. Sci.* **1999**, *442*, 291−299.

(24) Schaffner, M. H.; Patthey, F.; Schneider, W. D. *Surf. Sci.* **1998**, *417*, 159−167.

(25) Barbier, A.; Renaud, G.; Jupille, J. *Surf. Sci*. **2000**, *454*−*456*, 979−983.

(26) Stracke, P.; Krischok, S.; Kempter, V. *Surf. Sci.* **2001**, *473*, 86−96.

(27) Lagarde, P.; Colonna, S.; Flank, A. M.; Jupille, J. *Surf. Sci.* **2003**, *524*, 102−112.

(28) Abbet, S.; Ferrari, A. M.; Giordano, L.; Pacchioni, G.; Hakkinen, H.; Landman, U.; Heiz, U. *Surf. Sci.* **2002**, *514*, 249−255.

(29) Musolino, V.; Selloni, A.; Car, R. *Phys. Rev. Lett*. **1999**, *83*, 3242−3245.

(30) Musolino, V.; Selloni, A.; Car, R. *J. Chem Phys*. **1998**, *108*, 5044−5054.

(31) Musolino, V.; Del Corso, A.; Selloni, A. *Phys. Rev. Lett*. **1999**, *83*, 2761−2764.

(32) Musolino, V.; Selloni, A.; Car, R. *Surf. Sci.* **1998**, *402*−*404*, 413−417.

(33) Hakkinen, H.; Barnett, R. N.; Landman, U. *Phys. Rev. Lett*. **1999**, *82*, 3264−3267.

(34) Landman, U.; Luedtke, W. D. *Faraday Discuss.* **2004**, *125*, 1−22.

(35) Pileni, M.-P. *C. R. Chimie* **2003**, *6*, 965−978.

(36) Pileni, M. P.; Lalatonne, Y.; Ingert, D.; Lisiecki, I.; Coutry, A. *Faraday Discuss*. **2004**, *125*, 251−264.

(37) Shibata, T. *J. Am. Chem. Soc* **2002**, *124*, 11989−11996.

(38) Kreibig, U.; Vollmer, M. *Optical Properties of Metal Clusters*; Springer: Berlin, 1995.

(39) Sanchez, A.; Abbet, S.; Heiz, U.; Schneider, W. D.; Hakkinen, H.; Barnett, R. N.; Landman, U. *J. Phys. Chem. A* **1999**, *103*, 9573−9578.

(40) Hakkinen, H.; Landman, U. *J. Am. Chem. Soc*. **2001**, *123*, 9704−9705.

(41) Socaciu, L. D.; Hagen, J.; Bernhardt, T. M.; Woste, L.; Heiz, U.; Hakkinen, H.; Landman, U. *J. Am. Chem. Soc*. **2003**, *125*, 10437−10445.

(42) Del Vitto, A.; Sousa, C.; Illas, F.; Pacchioni, G. *J. Chem. Phys*. **2004**, *121*, 7457−7466.

(43) Garzon, I. L.; Beltran, M. R.; Gonzalez, G.; Gutierrez-Gonzales, I.; Michaelian, K.; Reyes-Nava, J. A.; Rodriguez-Hernandez, J. I. *Eur. Phys. J. D* **2003**, *24*, 105−109.

(44) Roman-Velasquez, C. E.; Noguez, C.; Garzon, I. L. *J. Phys. Chem. B*, **2003**, *107*, 12035−12038.

(45) Robach, O.; Renaud, G.; Barbier, A. *Surf. Sci*. **1998**, *401*, 227−235.

(46) *Progress in Experimental and Theoretical Studies of Clusters*; Kondow, T., Mafuné, F., Eds.; World Scientific: New York, 2003.

(47) Bravo-Perez, G.; Garzon, I. L.; Novaro, O. *THEOCHEM* **1999**, *493*, 225−231.

(48) Aprà, E.; Fortunelli, A. *J. Phys. Chem. A* **2003**, *107*, 2934−2942.

(49) Fortunelli, A.; Velasco, A. M. *THEOCHEM* **2002**, *586*, 17−27.

(50) Aprà, E.; Fortunelli, A. *THEOCHEM* **2000**, *501*−*502*, 251−259.

(51) Fortunelli, A. *THEOCHEM* **1999**, *493*, 233−240.

(52) Yannouleas, C.; Landman, U.; Herlert, A.; Schweikhard, L. *Phys. Rev. Lett*. **2001**, *86*, 2996−2999.

(53) Yoon, B.; Hakkinen, H.; Landman, U. *J. Phys. Chem. A* **2003**, *107*, 4066−4071.

(54) Hakkinen, H.; Landman, U. *Phys. Rev. B* **2000**, *62*, R2287−R2290.

(55) Cleveland, C. L.; Luedtke, W. D.; Landman, U. *Phys. Rev. B*, **1999**, *60*, 5065−507.7

(56) Wolf, M. D.; Landman, U. *J. Phys. Chem. A* **1998**, *102*, 6129−6137.

(57) Baletto, F.; Ferrando, R.; Fortunelli, A.; Montalenti, F.; Mottet, C. *J. Chem. Phys.* **2002**, *116*, 3856−3863.

(58) Baletto, F.; Mottet, C.; Ferrando, R. *Phys. Rev. Lett*. **2000**, *84*, 5544−5547.

(59) Baletto, F.; Mottet, C.; Ferrando, R. *Phys. Rev. B* **2002**, *66*, 1−11.

(60) Rossi, G.; Mottet, C.; Fortunelli, A.; Baletto, F.; Ferrando, R. *Phys. Rev. Lett*. **2004**, *93*, 105503.

(61) Garzon, I. L.; Kaplan, I. G.; Santamaria, R.; Novaro, O. *J. Chem. Phys*. **1998**, *109*, 2176−2184.

(62) Garzon, I. L.; Michaelian, K.; Beltran, M. R.; Posada-Amarillas, A.; Ordejon, P.; Artacho, E.; Sanchez-Portal, D.; Soler, J. M. *Phys. Rev. Lett.* **1998**, *81*, 1600−1603.

(63) Garzon, I. L.; Michaelian, K.; Beltran, M. R.; Posada-Amarillas, A.; Ordejon, P.; Artacho, E.; Sanchez-Portal, D.; Soler, J. M. *Eur. Phys. J. D* **1999**, *9*, 211−215.

(64) Michaelian, K.; Rendon, N.; Garzon, I. L. *Phys. Rev. B* **1999**, *60*, 2000−2010.

(65) Yudanov, I. V.; Vent, S.; Neyman, K.; Pacchioni, G.; Rosch, N. *Chem. Phys. Lett*. **1997**, *275*, 245−252.

(66) Neyman, K. M.; Vent, S.; Pacchioni, G.; Rosch, N. *Nuovo Cimento* **1997**, *19*, 1743−1748.

(67) Matveev, A. V.; Neyman, K. M.; Yudanov, I. V.; Rosch, N. *Surf. Sci*. **1999**, *426*, 123−139.

(68) Neyman, K. M., Inntam, C.; Nasluzov, V. A.; Kosarev, R.; Rosch, N. *Appl. Phys. A* **2004**, *78*, 823−828.

(69) Markovits, A.; Skalli, M. K.; Minot, C.; Pacchioni, G.; Lopez, N.; Illas, F. *J. Chem. Phys.* **2001**, *115*, 8172−8177.

(70) Menetrey, M.; Markovits, A.; Minot, C.; Del Vitto, A.; Pacchioni, G. *Surf. Sci*. **2004**, *549*, 294−304.

(71) Chiesa, M.; Paganini, M. C.; Giamello, E.; Di Valentin, C.; Pacchioni, G. *Angew. Chem., Int. Ed.* **2003**, *42*, 1759−1761.

(72) Pacchioni, G. *ChemPhysChem* **2003**, *4*, 1041−1047.

(73) Dominguez-Ariza, D.; Sousa, C.; Illas, F.; Ricci, D.; Pacchioni, G *Phys. Rev. B* **2003**, *68*, 054101.

(74) Ricci, D.; Di Valentin, C.; Pacchioni, G.; Sushko, P. V.; Shluger, A. L.; Giamello, E. *J. Am. Chem. Soc*. **2003**, *125*, 738−747.

(75) Ricci, D.; Pacchioni, G.; Sushko, P. V.; Shluger, A. L. *J. Chem. Phys*. **2002**, *117*, 2844−2851.

(76) Soave, R.; Ferrari, A. M.; Pacchioni, G. *J. Phys. Chem. B* **2001**, *105*, 9798−9804.

(77) Pacchioni, G. *Solid State Sci.* **2000**, 2, 161−179.

(78) Pacchioni, G.; Ferrari, A. M. *Catal. Today* **1999**, *50*, 533−540.

(79) Sousa, C.; Pacchioni, G.; Illas, F. *Surf. Sci*. **1999**, *429*, 217−228.

(80) Pacchioni, G.; Pescarmona, P. *Surf. Sci.* **1998**, *412/413*, 657−671.

(81) Pacchioni, G.; Ferrari, A. M.; Ieranò, G. *Faraday Discuss*. **1997**, *106*, 155−172.

(82) Giamello, E.; Paganini, M. C.; Murphy, D. M.; Ferrari, A. M.; Pacchioni, G. *J. Phys. Chem. B* **1997**, *101*, 971−982.

(83) Fucks, D.; Dorfman, S.; Kotomin, E. A.; Zhukovskii, Y. F.; Stoneham, M. *Phys. Rev. Lett*. **2000**, *85* (20), 4333−4336.

(84) Kuzovkov, V. N.; Popov, A. I.; Kotomin, E. A.; Monge, M. A.; Gonzalez, R.; Chen, Y. *Phys. Rev. B* **2001**, *64*, 1−5.

(85) Giordano, L.; Goniakowski, J.; Pacchioni, G. *Phys. Rev. B* **2001**, *75*, 1−9.

(86) Lopez, N.; Illas, F.; Rosch, N.; Pacchioni, G. *J. Chem. Phys*. **1999**, *110*, 4873−4879.

(87) Worz, A. S.; Judai, K.; Abbet, S.; Antonietti, J. M.; Heiz, U.; Del Vitto, A.; Giordano, L.; Pacchioni, G. *Chem. Phys. Lett.* **2004**, *399*, 266−270.

(88) Giordano, L.; Del Vitto, A.; Pacchioni, G.; Ferrari, A. M. *Surf. Sci*. **2003**, *540*, 63−75.

(89) Abbet, S.; Riedo, E.; Brune, H.; Heiz, U.; Ferrari, A. M.; Giordano, L.; Pacchioni, G. *J. Am. Chem. Soc*. **2001**, *123*, 6172−6178.

(90) Abbet, S.; Heiz, U.; Ferrari, A. M.; Giordano, L.; Di Valentin, C.; Pacchioni, G. *Thin Solid Films* **2001**, *400*, 37−42.

(91) Neyman, K.; Rosch, N.; Pacchioni, G. *Appl. Catal., A* **2000**, *191*, 3−13.

(92) Abbet, S.; Sanchez, A.; Heiz, U.; Schneider, W. D.; Ferrari, A. M.; Pacchioni, G.; Rosch, N. *J. Am. Chem. Soc*. **2000**, *122*, 3453−3457.

(93) Pacchioni, G.; Rosch, N. *J. Chem. Phys.* **1996**, *104*, 7329−7337.

(94) Neyman, K. M.; Vent, S.; Rosch, N.; Pacchioni, G. *Top. Catal*. **1999**, *9*, 153−161.

(95) Matveev, A. V.; Neyman, K. M.; Pacchioni, G.; Rosch, N. *Chem. Phys. Lett*. **1999**, *299*, 603−612.

(96) Ferrari, A. M.; Xiao, C.; Neyman, K. M.; Pacchioni, G.; Rosch, N.; *Phys. Chem. Chem. Phys*. **1999**, *1*, 4655−4661.

(97) Giordano, L.; Pacchioni, G.; Ferrari, A. M.; Illas, F.; Rosch, N. *Surf. Sci*. **2001**, *473*, 213−226.

(98) Giordano, L.; Pacchioni, G.; Illas, F.; Rosch, N. *Surf. Sci*. **2002**, *499*, 73−84.

(99) Di Valentin, C.; Giordano, L.; Pacchioni, G.; Rosch, N. *Surf. Sci.* **2003**, *522*, 175−184.

(100) Giordano, L.; Di Valentin, C.; Goniakowski, J.; Pacchioni, G. *Phys. Rev. Lett*. **2004**, *92*, 096105.

(101) Oviedo, J.; Sanz, J. F.; Lopez, N.; Illas, F. *J. Phys. Chem. B* **2000**, *104*, 4342−4348.

(102) Goniakowski, J. *Phys. Rev. B* **1998**, *58*, 1189−1192.

(103) Zhukovskii, Y. F.; Kotomin, E. A.; Fucks, D.; Dorfman, S. *Superlattices Microstruct.* **2004**, *36*, 63−72.

(104) Zhukovskii, Y. F.; Kotomin, E. A.; Jacobs, P. W. M.; Stoneham, A. M. *Phys. Rev. Lett*. **2000**, *84*, 1256−1259.

(105) Zhukovskii, Y. F.; Kotomin, E. A.; Fucks, D.; Dorfman, S.; Stoneham, A. M.; Sychev, O.; Borstel, G. *Appl. Surf. Sci*. **2004**, *226*, 298−305.

(106) Zhukovskii, Y. F.; Kotomin, E. A.; Fucks, D.; Dorfman, S. *Surf. Sci*. **2004**, *566−568*, 122−129.

(107) Zhukovskii, Y. F.; Kotomin, E. A.; Jacobs, P. W. M.; Stoneham, A. M.; Harding, J. H. *J. Phys: Condens. Matter* **2000**, *12*, 55−66.

(108) Zhukovskii, Y. F.; Kotomin, E. A. *Phys. Status Solidi* **2005**, *2*, 347−350.

(109) Herschend, B.; Hermansson, K.; Alfredsson, M.; Zhukovskii, Y. F.; Kotomin, E. A.; Jacobs, P. W. M. *J. Phys. Chem. B* **2003**, *107*, 11893−11899.

(110) Fucks, D.; Dorfman, S.; Zhukovskii, Y. F.; Kotomin, E. A.; Stoneham, A. H. *Surf. Sci.* **2002**, *499*, 24−40.

(111) Vervisch, W.; Mottet, C.; Goniakovskii, J. *Phys. Rev. B* **2002**, *65*, 245411.

(112) Vervisch, W.; Mottet, C.; Goniakovskii, J. *Eur. Phys. J. D* **2004**, *24*, 311−314.

(113) Mottet, C.; Goniakovskii, J. *Surf. Sci*. **2004**, *566*−*568*, 443−450.

(114) Baroni, S.; Del Corso, A.; de Gironcoli, S.; Giannozzi, P. *PWscf*; Scuola Internazionale Superiore di Studi Avanzati and DEMOCRITOS National Simulation Center: Trieste, Italy. http://www.pwscf.org.

(115) Perdew, J. P.; Chevary, J. A.; Vosko, S. H.; Jackson, K. A.; Pederson, M. R.; Singh, D. J.; Fiolhais, C. *Phys. Rev. B* **1992**, *46*, 6671−6687.

(116) Fortunelli, A. *J. Phys. Chem.* **1995**, *99*, 9056−9061.

(117) Del Vitto, A.; Pacchioni, G.; Delbecq, F.; Sautet, P. *J. Phys. Chem. B* **2005**, 109, 8040−8048.

CT050073E